Journal of Alloys and Compounds 509 (2011) 4525–4529

Contents lists available at ScienceDirect

Journal of Alloys and Compounds

journal homepage: www.elsevier.com/locate/jallcom

Structural and optical study of samarium doped cerium oxide thin films prepared by electron beam evaporation

M.S. Anwar, Shalendra Kumar, Nishat Arshi, Faheem Ahmed, Y.J. Seo, C.G. Lee, Bon Heun Koo*

School of Nano and Advanced Materials Engineering, Changwon National University, Changwon, # 9 Sarim Dong, Gyeongnam, 641-773, Republic of Korea

ARTICLE INFO

Article history:
Received 20 October 2010
Received in revised form 7 January 2011
Accepted 7 January 2011
Available online 15 January 2011

Keywords:
CeO_2
XRD
Defects
Raman spectra
Fuel cell
Thin films

ABSTRACT

Samarium doped cerium oxide films were grown on the glass substrate using e-beam deposition technique and then characterized using different techniques: X-ray diffraction (XRD), field emission scanning electron microscopy (FE-SEM), Raman spectroscopy and UV–visible spectroscopy measurements. XRD analysis shows that all the films have cubic structure and the crystallite size decreases from 18 to 13 nm as the samarium (Sm) concentration increases. The FE-SEM images indicate that all the films have columnar growth. UV–visible measurements reflect that the films have high transparency (>80%) in the visible region. From the Raman spectra, we have observed two peaks at 466 and 565 cm^{-1}. The peak at 466 cm^{-1} is assigned to the F_{2g} mode of cerium oxide (CeO_2) whereas the peak at 565 cm^{-1} is due to the presence of the oxygen vacancies. The increase in the intensity of the peak at 565 cm^{-1} indicates that the oxygen vacancy increases with Sm doping.

1. Introduction

The materials having high oxygen ion conductivity are impelled by a number of important applications, such as solid oxide fuel cells (SOFCs) and oxygen sensors [1–5]. A number of studies have shown that materials with grain size less than 100 nm exhibit optical, electrical, catalytic and mechanical properties that are different than those observed for bulk materials [6–9]. These possibilities have created a new challenge for research in ion-conductive materials such as cerium oxide. CeO_2 and CeO_2 based compounds have been extensively studied and employed in various applications including catalysts, oxygen permeation membrane systems, polishing materials and UV blockers [10–13]. In particular, the high ionic conductivity of doped CeO_2 makes it an attractive and potential electrolyte for SOFCs that operated at lower temperatures as compared to conventional SOFCs employing doped zirconium oxide as the electrolyte and operating above 800 °C [14–19]. Currently, this high operation temperature for SOFCs limits the full developments of these environmental friendly high-efficiency electrical power generating systems. One of the ways for lowering the working temperature and increasing the performance of SOFCs is to use the thinner layers of electrolytes with high oxygen vacancies. Because in these electrolytes, the current is carried by oxygen ions that are transported by oxygen vacancies, present to compensate for the lower charge of the dopants cations. Moreover, thinner and optimum grain size electrolytes are needed to reduce the resistance to ionic transport [20]. The extensive study have been done on oxygen-ion conductivities of CeO_2-based electrolytes doped with various rare earth ions (La^{3+}, Sr^{2+}, Y^{3+}, Sm^{3+} and Gd^{3+}) at different concentrations [15,16]. Among them samarium (Sm^{3+}) doped CeO_2 was found to exhibit the highest oxygen-ion conductivity at certain fixed doping level [17,18].

Many research papers have been reported about the optical properties of CeO_2 films. The CeO_2 based films have high refractive index (between 1.6 and 2.4), dc permittivity and transparency in the visible and, near- and mid-IR [21–25]. The direct band gap of CeO_2 films varies between 3.2 and 3.6 eV. However, a higher value up to 4.14 eV is also reported for different nanostructures of cerium oxide [25–28]. Due to these interesting properties, CeO_2 based films have been also proposed for optical, microelectronics and optoelectronic device applications [29,30]. Several techniques have been used to deposit CeO_2 based films such as: tape casting, screen printing, spin coating, sol–gel, chemical vapour deposition, sputtering and electron beam evaporation [10–13,22]. Among these, physical vapour processing methods are good for making very thin and dense films with controlling their thickness, porosity, crystalline structure and other parameters.

In the present study samarium doped cerium oxide thin films were deposited by electron beam evaporation technique. The aim

* Corresponding author. Fax: +82 55 262 6486.
E-mail addresses: shafiqueamu@gmail.com (M.S. Anwar), bhkoo@changwon.ac.kr (B.H. Koo).

0925-8388/$ – see front matter © 2011 Elsevier B.V. All rights reserved.
doi:10.1016/j.jallcom.2011.01.067

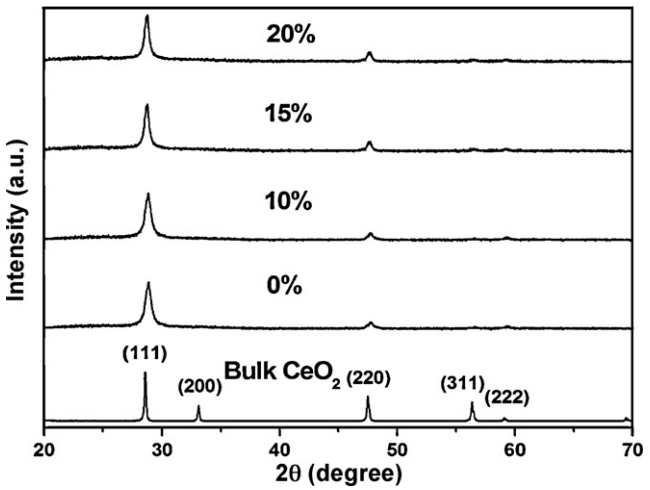

Fig. 1. Diffraction patterns of SDCO thin films deposited on glass substrate at substrate temperature of 300 °C.

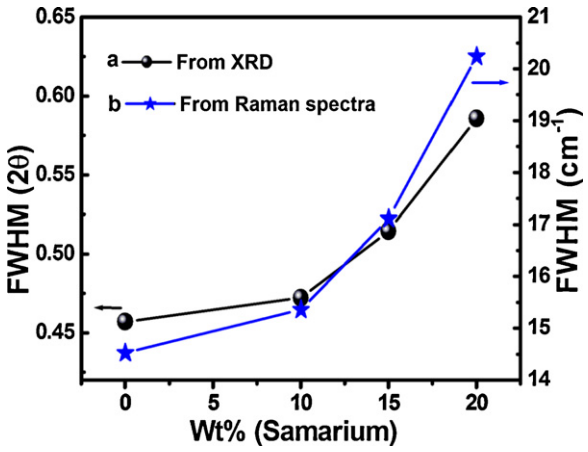

Fig. 2. Full width at half maximum (FWHM) of SDCO thin films: (a) from XRD; (b) from Raman spectra.

of this work is to study the influence of samarium doping on the characteristics such as: structure, grain size, morphology, vacancy formation and optical properties.

2. Experimental details

Samarium doped CeO_2 (SDCO) thin films were prepared by e-beam deposition technique on glass substrates in a high vacuum chamber (base pressure $\sim 10^{-6}$ Torr). The substrates were cleaned in an ultrasonic bath (in pure acetone) for 15 min and then washed with distilled water. Finally, their surface was dried by blow of Argon gas. High purity (99.99%, Aldrich) CeO_2 and samarium oxide (99.99%, Aldrich) were used in this experiment. The SDCO powders were prepared by conventional solid state reaction technique and used as the evaporation material. Before deposition, SDCO powders were pressed into pellets and sintered at 1200 °C for 12 h. The distance between the substrate and target was fixed at ~45 cm to obtain a uniform thickness of the films. The films were deposited at substrate temperature of 300 °C for 40 min. A constant substrate temperature and e-beam gun power of 0.40 kW were chosen to study the influence of samarium doping on the morphology, structure, defects and optical properties of the as deposited films.

The film structure was analyzed using a X-ray diffractometer (Rigaku MiniFlex II) operating with *Cu* K_α ($\lambda = 1.5406$ Å, 30 kV, 15 mA) radiation. A typical scan range of 20–70° (2θ) and a step size of 0.02° (2θ) were used. The crystallite size (D) of SDCO films were

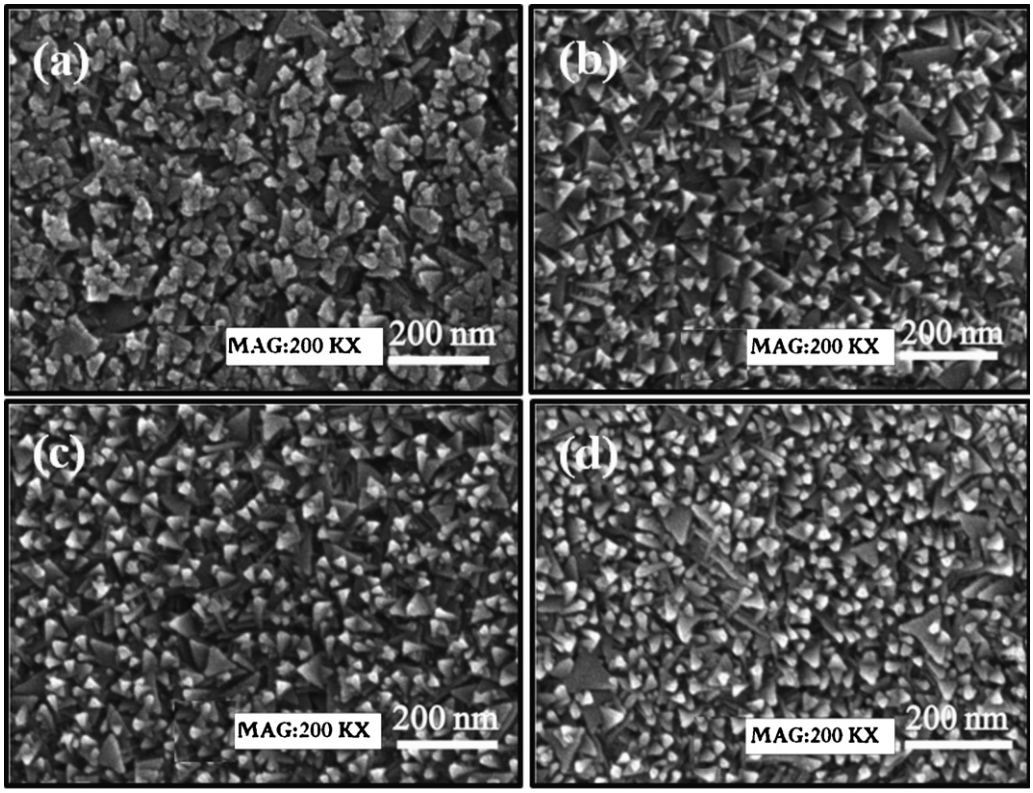

Fig. 3. SEM picture of the surface of SDCO thin films deposited at substrate temperature of 300 °C: (a) 0% Sm; (b) 10% Sm; (c) 15% Sm; (d) 20% Sm.

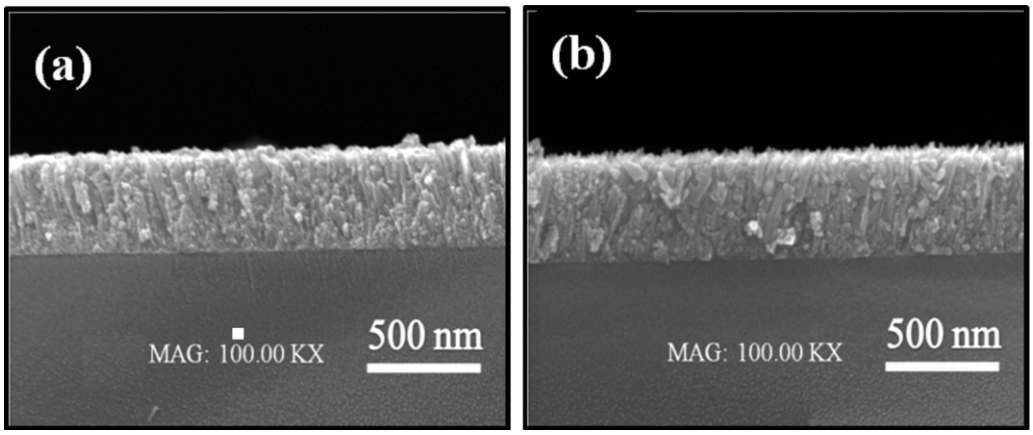

Fig. 4. SEM picture of the cross section of SDCO thin films deposited at substrate temperature of 300 °C: (a) 10% Sm; (b) 20% Sm.

calculated using Scherrer's equation [31]:

$$D_{hkl} = \frac{0.9\lambda}{B_{hkl}\,Cos\,\theta_{hkl}} \quad (1)$$

where λ is the wavelength of the radiation, θ_{hkl} is the diffraction angle, and B_{hkl} is the full width at half maximum of the (*hkl*) diffraction peak. A field emission scanning electron microscope (FE-SEM) (TESCAN; MIRA II LMH, 30 kV) was used to investigate the morphology and thickness of SDCO thin films. The Raman spectra were recorded using a micro-Raman spectrometer (NRS-3100) with a 514.5 nm Ar^+ laser as an excitation source in the backscattering configuration at room temperature. The spectral resolution was 1 cm^{-1}.The optical properties of the films were investigated using an UV–VIS–NIR light spectrophotometer (JASCO, V570) in transmission mode.

3. Results and discussion

Fig. 1 shows the XRD patterns of the prepared SDCO thin films. All the diffraction patterns of the samples correspond to the fluorite cubic structure of SDCO (JCPDS Card No. 89-8436, 75-0157 and 75-0158 for 0, 10 and 20 wt% of samarium doping respectively) with Fm3m space group. No evidence of any other secondary phase was detected for all the samples. It shows well doping of samarium in host matrix without any impurity peaks. For comparison, XRD pattern for bulk CeO_2 was also plotted. It is observed that all films show polycrystalline behavior with maximum intensity for the (1 1 1) peak when cubic phase SDCO pellets used as evaporation material. As deposited SDCO thin films repeat the crystal structure for all doping concentrations and keeps cubic (1 1 1) as highest intensity peak. Fig. 2 shows FWHM (full width at half maximum) observed from the (1 1 1) XRD peak and (466 cm^{-1}) Raman peak for all films. The FWHM increases as the samarium concentration increases. The crystallite size decreases from 18 to 13 nm as the doping (Sm) increases.

Fig. 3 represents the FE-SEM image of Sm doped CeO_2 films. It is observed that the Sm doping affects the crystallite size of the films. It can be seen from the FE-SEM micrograph that the grains have triangular shape. In order to see more insight of the growth, we have performed cross-sectional FE-SEM measurement of the Sm doped CeO_2 films as shown in Fig. 4. It is found that most of the columnar grains are oriented in the direction-perpendicular to the substrate with small gaps in between. The surface morphology is more clear in case of 20% Sm doped CeO_2 film as compared to pure CeO_2 film. A slight compact and dense structure is observed with 20% of Sm doping (Fig. 3). The incorporation of Sm in the CeO_2 thin films leads to a change in structure and surface morphology of the films, as can be seen from Figs. 3 and 4. Similar observations were also found in the formation of doped CeO_2 thin films in earlier report [32].

Raman scattering was investigated in order to carefully identify the lattice disorder. Fig. 5(a) shows the Raman spectra of nanocrystalline SDCO thin films compared with the spectrum of a pure CeO_2 film. The main peak was observed at 466 cm^{-1} for pure CeO_2 film, which is attributed to a symmetrical stretching mode (F_{2g}) of the Ce–O8 vibrational unit [33]. If there is any disorder in the oxygen sublattice, this mode should be influenced by a broadening

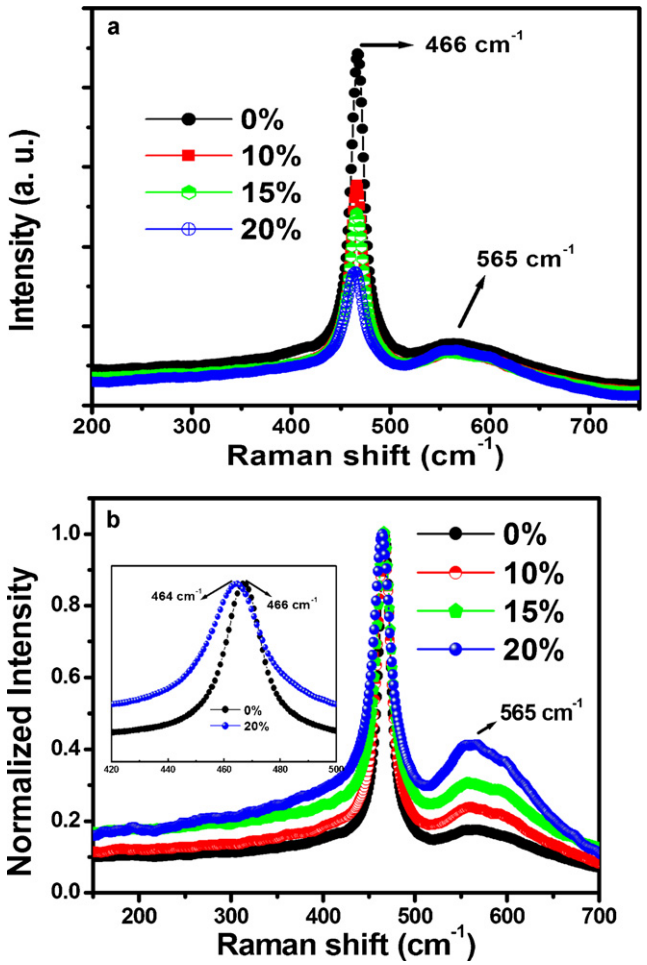

Fig. 5. Raman spectra of (a) SDCO thin films; (b) normalized.

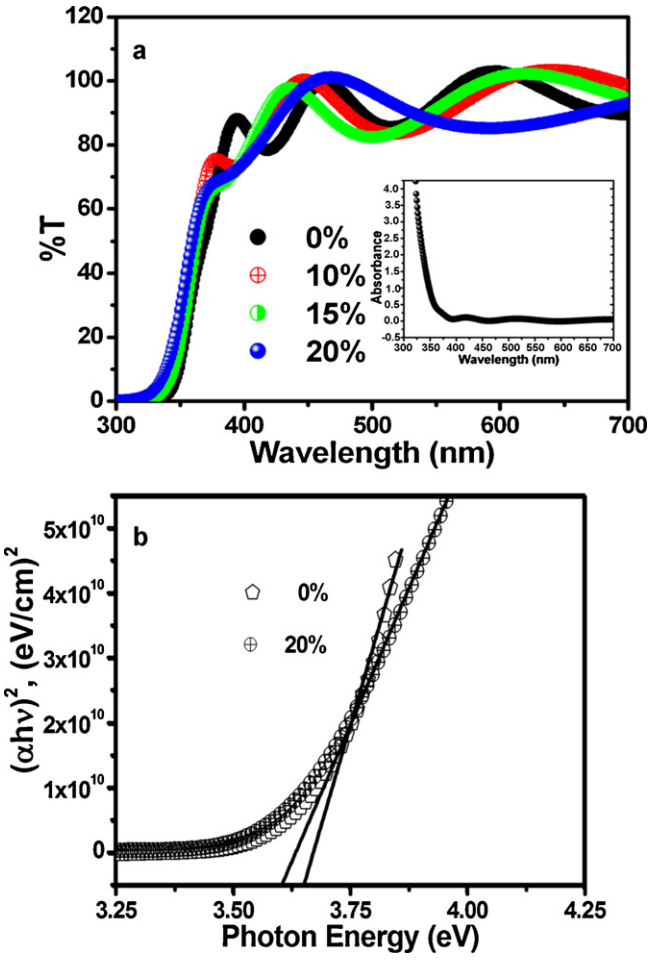

Fig. 6. (a) UV–visible spectra of SDCO thin films; (b) plots of $(\alpha h\nu)^2$ versus photon energy (eV) for the pure CeO_2 film and 20% Sm doped.

of the line and an increase in its asymmetry which is attributed to reduction of the phonon lifetime in the nanocrystalline regime [34]. Fig. 2 shows the FWHM (line broadening of F_{2g} mode) of SDCO films increases in comparison with that of pure CeO_2 film, which corresponds well to common features of the rare earth-doping (La, Pr, Nd and Gd) effect on the F_{2g} band. The Raman line broadening can be described by the dependence of its FWHM upon the grain size. The FWHM of the Raman line is inversely proportional to the grain size. Fig. 5(b) shows line broadening on both the low and high frequency sides with increasing Sm doping, which reveals that the grain size decreasing with the increase in Sm doping. These results are very well matched with the XRD results of all deposited SDCO films.

The normalized Raman spectra presented in Fig. 5(b), clearly show an additional Raman band at 565 cm^{-1} which corresponds to oxygen vacancies formed by a trivalent dopant [35]. Mcbride et al. [35] reported that the qualitative trends in Raman spectra for lanthanides doped CeO_2 are the same for all dopants and the intensity of the Raman peak at 570 cm^{-1} for La-doped CeO_2 increases uniformly with La doping. In the present work, it can be seen that the intensity of defects induced band in the spectra increases with the Sm^{3+} doping, but only after the spectra are normalized with respect to the integrated F_{2g} mode strength. Thus, the oxygen vacancies can be controlled in the CeO_2 matrix by variation of Sm doping concentration. It also confirmed the possibility of incorporation of Sm in a CeO_2 matrix as previously indicated by the XRD analysis.

UV–visible measurements have been carried out to investigate the optical properties. Fig. 6(a) shows the transmittance spectra of SDCO films. All films have high (>80%) transmittance in the visible region of the spectrum. Also, it was observed that there is no transmittance at wavelengths lower than 300 nm. Inset of Fig. 6(a) shows the UV–visible absorption pattern of pure CeO_2 thin film. From the absorption data the band gap energy (E_g) of these films was calculated using the Tauc's equation:

$$ah\nu = A(h\nu - E_g)^n \quad (2)$$

where α is absorption coefficient and n is a constant which depends on the probability of transition; it takes the values 1/2, 3/2, 2, and 3 for direct allowed, direct forbidden, indirect allowed, and indirect forbidden transitions, respectively. Fig. 6(b) shows the variation of $(\alpha h\nu)^2$ versus $h\nu$, which is a straight line in the higher energies domain, indicating a direct optical transition. The band gap energy E_g is obtained by extrapolating the linear portion of the graph to energy axis at $\alpha = 0$. For the direct band gap, the values are between 3.2 and 3.5 eV, in agreement with the literature [25,30,36]. These values are slightly lower than those reported by Guo et al. [36] and Murali [37], who observed values between 3.53 and 3.6 eV. In contrast, much higher values were observed by Zhang et al. [28] and Tsunekawa et al. [38], up to 3.95 and 4.17, respectively. These authors explain such high values by quantum confinement effects for nanorods and nanoparticles, respectively. In our case, the result shows that the band gap reduces from 3.65 eV for un-doped CeO_2 thin film to 3.58 eV for 20% Sm doped CeO_2 thin film. This decrease in the band gap may be attributed to the more oxygen vacancies present in the 20% Sm doped CeO_2 thin film.

4. Conclusions

Effect of Sm doping on morphology, structural and optical properties of the CeO_2 thin films deposited by e-beam evaporation on glass substrate at 300 °C was investigated. The XRD results show that as deposited SDCO films are cubic with dominating orientation (1 1 1) and reproduce the crystal structure of the chosen evaporated material. Crystallite size decreases from 18 nm to 13 nm, when Sm doping was increased from 0 to 20 wt%. The analysis of normalized Raman spectra revealed that, the intensity of the Raman band found at 565 cm^{-1} (due to oxygen vacancies) increases with Sm doping. The peak corresponding to F_{2g} mode of CeO_2 is broadened and blue shifted with incorporation of Sm in CeO_2 films. FE-SEM images showed change in morphology of the films with doping and optical studies showed >80% transparency in the visible region with reduction in band gap from 3.65 eV for pure CeO_2 to 3.58 eV for 20% Sm doped thin film.

Acknowledgments

This research was supported by the MKE (The Ministry of Knowledge Economy), Korea, under the ITRC (Information Technology Research Center) support program supervised by the NIPA (National IT Industry Promotion Agency) (NIPA-2010-C1090-1021-0015).

References

[1] F.-Y. Wang, B.-Z. Wan, S. Cheng, J. Solid State Chem. 9 (2005) 168.
[2] Y. Zheng, M. Zhou, L. Ge, S. Li, H. Chen, L. Guo, J. Alloys Compd. 509 (2011) 1244.
[3] H.-J. Ahn, J.-S. Jang, Y.E. Sung, T.-Y. Seong, J. Alloys Compd. 473 (2009) L28.
[4] L. Zhang, J. Gao, M. Liu, C. Xia, J. Alloys Compd. 482 (2009) 168.
[5] L. Jia a b, M. Shen, J. Wang, W. Gu, J. Alloys Compd. 473 (2009) 293.
[6] S.A. Hassanzadeh-Tabrizi, M. Mazaheri, M. Aminzare, S.K. Sadrnezhaad, J. Alloys Compd. 491 (2010) 499.
[7] M.-N. Guo, C.-X. Guo, L.-Y. Jin, Y.-J. Wang, J.-Q. Lu, M.-F. Luo, Mater. Lett. 64 (2010) 1638.
[8] B.B. Patil, S.H. Pawar, J. Alloys Compd. 509 (2011) 414.
[9] G. Wang, Q. Mu, T. Chen, Y. Wang, J. Alloys Compd. 493 (2010) 202.
[10] X. Liu, K. Zhou, L. Wang, B. Wang, Y. Li, J. Amer. Chem. Soc. 131 (2009) 3140.

[11] G. Yi Hongwei Yang, B. Li, H. Lin, K.-i. Tanaka, Y. Yuan, Catal. Today 157 (2010) 83.
[12] L. Chen, J. Li, M. Ge, R. Zhu, Catal. Today 153 (2010) 77.
[13] P. Jasinski, T. Suzuki, U.A. Harlan, Sensors Actuators B 95 (2003) 73.
[14] M. Liu, C. He, J. Wang, W.G. Wang, Z.w. Wang, J. Alloys Compd. 502 (2010) 319.
[15] Y.-P. Fu, S.-H. Chen, Ceram. Int. 36 (2010) 483.
[16] B.C.H. Steele, Solid State Ionics 129 (2000) 95.
[17] V.V. Khartona, F.M.B. Marques, A. Atkinson, Solid State Ionics 174 (2004) 135.
[18] K. Singh, S.A. Acharya, S.S. Bhoga, Ionics 13 (2007) 429.
[19] Steele, C.H. Brian, Heinzel, Angelika, Nature 414 (2001) 345.
[20] B. Dalslet, P. Blennow, P. Vang Hendriksen, N. Bonanos, D. Lybye, M. Mogensen, J.Solid State Electrochem. 10 (2006) 547.
[21] E.E. Khawaja, S.M.A. Durrani, M.F. Al-Kuhaili, J. Phys. D: Appl. Phys. 36 (2003) 545.
[22] Catalina Mansilla, Solid State Sci. 11 (2009) 1456.
[23] E.C.C. Souza, H.F. Brito, E.N.S. Muccillo, J. Alloys Compd. 491 (2010) 460.
[24] Y. Jiang, N. Bahlawane, J. Alloys Compd. 485 (2009) L52.
[25] P. Patsalas, S. Logothetidis, L. Sygellou, S. Kennou, Phys. Rev. B 68 (2003).
[26] X. Lu, X. Li, F. Chen, C. Ni, Z. hen, J. Alloys Compd. 476 (2009) 958.
[27] B. Liu, B. Liu, Q. Li, Z. Li, R. Liu, X. Zou, W. Wu, W. Cui, Z. Liu, D. Li, BoZou, T. Cui, G. Zou, J. Alloys Compd. 503 (2010) 519.
[28] D.E. Zhang, X.M. Ni, H.G. Zheng, X.J. Zhang, J.M. Song, Solid State Sci. 8 (2006) 1290.
[29] S. Logothetidis, P. Patsalas, E.K. Evangelou, N. Konofaos, I. Tsiaoussis, N. Frangis, Mater. Sci. Eng. B 109 (2004) 69.
[30] P. Patsalas, S. Logothetidis, C. Metaxa, Appl. Phys. Lett. 81 (2002) 466.
[31] B.B. Patil, S.H. Pawar, Appl. Surf. Sci. 253 (2007) 4994.
[32] C. Mansilla, J.P. Holgado, J.P. Espinós, A.R. González-Elipe, F. Yubero, Surf. Coat. Technol. 202 (2007) 1256.
[33] I. Kosacki, Toshio Suzuki, Harlan U. Anderson, Philippe Colomban, Solid State Ionics 149 (2002) 99.
[34] S. Wang, W. Wang, J. Zuo, Y. Qian, Mater. Chem. Phys. 68 (2001) 246.
[35] J.R. McBride, K.C. Hass, B.D. Poindexter, W.H. Weber, J. Appl. Phys. 76 (1994) 2435.
[36] S. Guo, H. Arvin, S.N. Jacobsen, K. Jarrendahl, U. Helmersson, J. Appl. Phys. 77 (1995) 5369.
[37] K.R. Murali, J. Mater. Sci.: Mater. Electron. 19 (2008) 369.
[38] S. Tsunekawa, J.T. Wang, Y. Kawazoe, A. Kasuya, J. Appl. Phys. 94 (2003) 3654.